Journal of proteome research

pubs.acs.org/jpr

Article

Messages from the Small Intestine Carried by Extracellular Vesicles in Prediabetes: A Proteomic Portrait

Inês Ferreira,[¶] Rita Machado de Oliveira,[¶] Ana Sofia Carvalho, Akiko Teshima, Hans Christian Beck, Rune Matthiesen, Bruno Costa-Silva,[*,¶] and Maria Paula Macedo[*,¶]

Cite This: *J. Proteome Res.* 2022, 21, 910−920

Read Online

ACCESS | Metrics & More | Article Recommendations | Supporting Information

ABSTRACT: Extracellular vesicles (EVs) mediate communication in physiological and pathological conditions. In the pathogenesis of type 2 diabetes, inter-organ communication plays an important role in its progress and metabolic surgery leads to its remission. Moreover, gut dysbiosis is emerging as a diabetogenic factor. However, it remains unclear how the gut senses metabolic alterations and whether this is transmitted to other tissues via EVs. Using a diet-induced prediabetic mouse model, we observed that protein packaging in gut-derived EVs (GDE), specifically the small intestine, is altered in prediabetes. Proteins related to lipid metabolism and to oxidative stress management were more abundant in prediabetic GDE compared to healthy controls. On the other hand, proteins related to glycolytic activity, as well as those responsible for the degradation of polyubiquitinated composites, were depleted in prediabetic GDE. Together, our findings show that protein packaging in GDE is markedly modified during prediabetes pathogenesis, thus suggesting that prediabetic alterations in the small intestine are translated into modified GDE proteomes, which are dispersed into the circulation where they can interact with and influence the metabolic status of other tissues. This study highlights the importance of the small intestine as a tissue that propagates prediabetic metabolic dysfunction throughout the body and the importance of GDE as the messengers. Data are available via ProteomeXchange with identifier PXD028338.

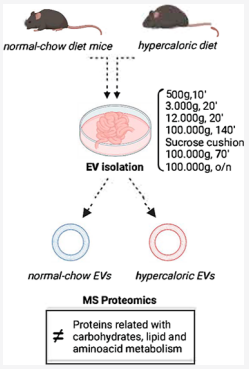

KEYWORDS: *small intestines, extracellular vesicles, type 2 diabetes, lipids, diet*

INTRODUCTION

Type 2 diabetes (T2D) is the most common chronic metabolic disease characterized by high blood glucose and it accounts for 95% of diabetes cases in adulthood.[1] The escalating incidence of T2D as a consequence of sedentary lifestyle and over-nutrition imposes a substantial burden to healthcare systems worldwide. Among the therapeutic interventions, metabolic surgery which targets the small intestine is the most effective procedure in diabetes remission.[2,3] Prediabetes is a high-risk state for T2D, and it is defined by glycaemic levels higher than normal but lower than diabetic limits.[4] This stage can be seen as a fork in the road, and if left untreated, the likelihood for progression to diabetes is high. Importantly, with timely diagnosis and with patient's compliance to lifestyle intervention, prediabetes can be reversed.[5] Obesity is a potent risk factor for diabetes. Moreover, a diet rich in fat and sugar, with large intake of finely processed grains and starchy carbohydrates is directly associated with this disease.[6]

Blood glucose homeostasis requires a constant communication between insulin-secreting and insulin-sensitive organs. Failure in the coordination between these organs can lead to a rise in blood glucose levels and to prediabetes. Recently, extracellular vesicles (EVs) emerged as an important component of organismal communication and have been implicated in the pathophysiology of diabetes.[7] These small vesicles are able to transfer proteins and nucleic acids from a releasing cell to a distant target cell, thus modulating gene and protein expression and leading to functional changes.[8,9] Interestingly, visceral adipose tissue-derived EVs trigger systemic inflammation, glucose intolerance, and insulin resistance; hallmarks of prediabetes.[10] In obese patients, adipose tissue-EVs were able to modulate insulin responses in hepatocytes and muscle cells.[11] Impressively, a recent study with nonalcoholic fatty liver disease patients suggests that levels of total and hepatocyte-derived EVs correlate with disease severity, opening up the door for the usage of EV-based protein-liquid biopsies.[12]

The intestinal system is daily exposed to food, millions of pathogens, and high concentrations of foreign antigens. In the case of the gut EVs, the composition and effects of EVs released by the resident microbiota have been explored.[13,14] For instance, these EVs are released into the gut mucosa and participate in local innate responses to invading bacteria through microbicidal activity[15] and mediate gut permeability through the regulation of tight junctions.[16] While the

Received: May 11, 2021
Published: March 9, 2022

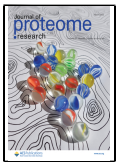

contribution of microbiota is crucial to maintain intestinal homeostasis, the epithelial cells are a critical component of the intestinal defense system forming a selective permeable barrier, allowing the absorption of nutrients, electrolytes and water, and blocking ingress of toxins and antigens. Epithelial cells in the gut were described to secrete EVs which play a role as antigen-carrying structures.[17] Whether EVs derived from the small intestine play a primordial role as a diabetogenic trigger needs to be elucidated. Indeed, the relevance of the gastrointestinal tract in diabetes is elucidated by the fact that metabolic surgery improves glucose homeostasis more effectively than any known pharmaceutical or behavioral approach, causing durable remission in many patients with T2D.[18] Attempts to elucidate the exact mechanism by which gastro-intestinal surgery reverses T2D have implicated changes in the gut hormones, bile acid metabolism, intestinal nutrient sensing and metabolism, gut microbiota, and other factors.[19] Gut dysbiosis recently emerged as a possible player in the development of T2D.[20,21] Despite the literature on the impact of microbiota in T2D onset and development, the role of the small intestine EVs, independent of EVs derived from the biota, is still elusive. While gut-derived EVs (GDEs) are considered to play an important role in intestinal diseases, it is not known how GDE protein content is modulated by a western diet. Therefore, it is timely to understand the importance of the small intestine as a metabolically active organ in prediabetes and the means by which it communicates with other tissues via EVs. Here, we aim at characterizing the differences in GDE proteome of diet-induced prediabetic mice compared to that of healthy mice fed a standard chow diet.

RESULTS

Description of the Prediabetic Mouse Model

First, we established a mouse model that recapitulates many features of prediabetes.[22] High fat and sugar feeding leads to obesity, hyperinsulinemia, and glucose intolerance. Therefore, we used an hypercaloric diet (HD) with a composition of 58% fat and 18% sucrose, in contrast with normal-chow diet (NCD) that is 11% fat with no added sugar. After 12 weeks of diet, HD mice demonstrate significantly increased body weight (Figure 1A,B) and an abnormal intrahepatic fat accumulation—a hallmark of liver steatosis (Figure 1C). They also developed glucose intolerance, evaluated by a glucose tolerance test in the previous week of sacrifice and correspondent area under the curve for each group (Figure 1D,E).

Characterization of Intestine-Derived Extracellular Vesicles

Once the prediabetic phenotype was validated in the diet-induced obese animals, we evaluated the presence of EVs in the small intestine. We stained small intestine cross sections for CD81, a commonly used EV-marker, and the presence of this protein was detected in similar levels in the lumen of the intestine under both conditions (NCD- and HD-fed mice—Figure 1F). Moreover, western blot was performed to confirm the enrichment of CD63, a commonly used EV marker, in GDE from NCD and HD when compared with the tissue (Figure 1G). Next, GDEs were characterized by nanoparticle tracking analysis, and the total amount of protein was quantified by BCA. The mean size of the particles, in both conditions, was around 100 nm (NCD = 152.8 ± 67.5; HD = 128.6 ± 50.7) (Figure 1H). While the number of EVs is decreased in HD animals (Figure 1I), protein cargo was higher

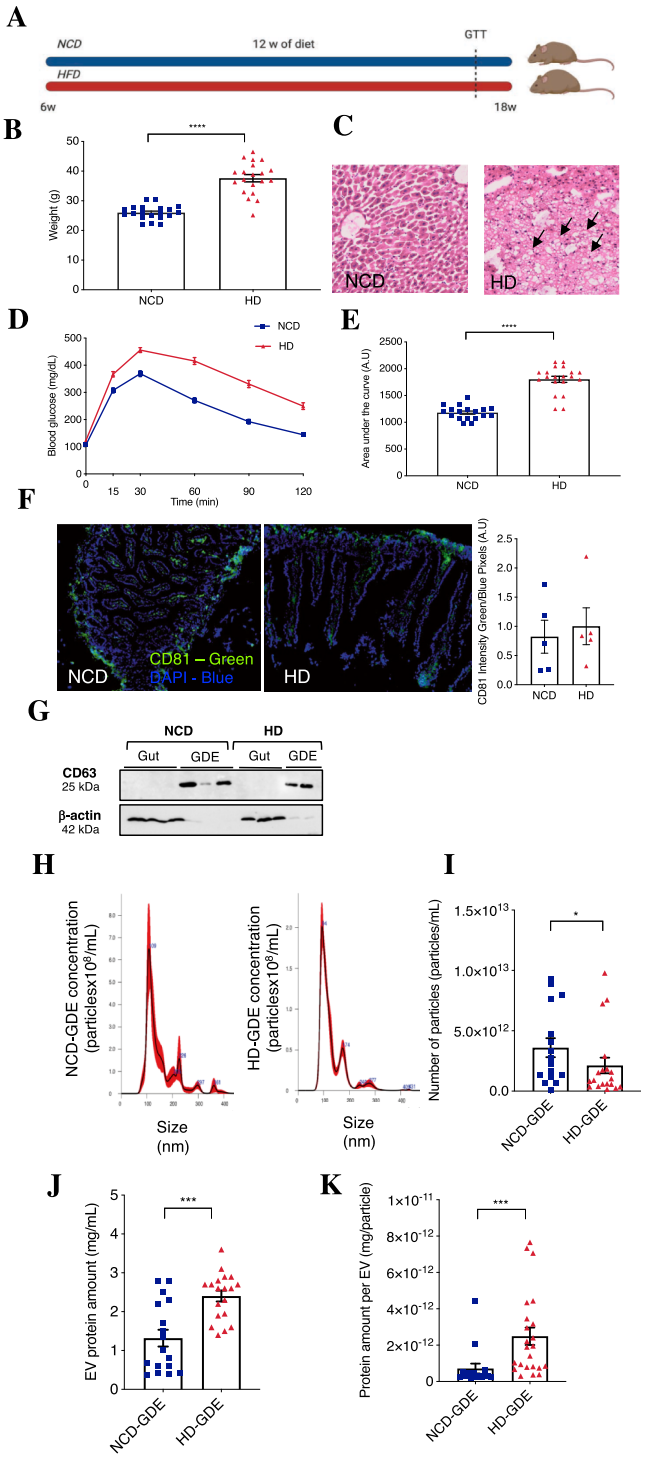

Figure 1. High-fat diet induces prediabetes in mice and increases protein cargo in GDE. (A) Diet plan schematic representation. (B) Body weight (n = 20 per group). (C) Representative hematoxylin–eosin images of liver histological sections of NCD and HD mice. White areas indicated by black arrows are lipid droplets, revealing steatosis in the liver of mice subjected to HD. (D) Plasma glucose profile (md/dL) along a glucose tolerance test (GTT) at different time points after glucose bolus (0, 15, 30, 60, 90, and 120 min) at week 17 of age. (E) Mean area under the curve of the GTT. Results are expressed as mean ± SEM; n = 20 per group. Unpaired t-test with Welch's correction for (B,D); ****p < 0.0001. (F) Gut cross sections, EVs are labeled in green (CD81) and nuclei in blue (DAPI). NCD gut tissue in the left and HD gut tissue in the right. CD81 quantification in the gut. (G) Immunoblotting of gut tissue and GDE

https://doi.org/10.1021/acs.jproteome.1c00353
J. Proteome Res. 2022, 21, 910–920

Figure 1. continued

isolated from NCD and HD mice. Protein extracts prepared from gut (10 μg) and from GDE (15 μg) were analyzed by western blotting using antibodies against EV marker CD63 and β-actin. (H) Size and concentration distribution of GDE determined by nanoparticle tracking analysis (NTA). A representative NTA graph of GDE of mice fed with NCD (NCD-EV) (left) and HD (HD-EV) (right). (I) Analysis of the number of particles per milliliter of sample. (J) Protein quantification in GDE in milligram per milliliter of sample, obtained by BCA. (K) Protein content per GDE, represented in milligram of protein per particle. Results are expressed as mean ± SEM; n = 17 for NCD-EV and n = 25 for HD-EV. Unpaired t-test with Welch's correction (F,I–K); ***p < 0.0005, **p < 0.005.

in GDE isolated from HD-fed mice (HD-GDE) than in NCD-fed (NCD-GDE) mice (Figure 1J). Interestingly, the amount of protein per GDE was higher in prediabetic mice than in controls (Figure 1K).

Proteomics Study

EV protein cargo provides valuable information regarding the cellular environment where they are produced.[23] We proposed that a diet induced dysmetabolic environment modulates the protein composition of GDE. Thus, to identify the impact of the diet-induced prediabetic gut milieu on GDE protein cargo, we isolated GDE (Figure S2) from mice under HD and respective controls and analyzed it by mass spectrometry (MS) (Figure S2A). Potential contribution of gut bacteria EVs was ruled out by MS analysis, which showed the absence of bacterial proteins (Figure S2B), and culture of gut conditioned media in antibiotics-free agar, which did not display bacterial growth (Figure S2C).

Bioinformatic Analysis of the MS Identified Proteins

After filtering the identified proteins for reverse proteins used for false discovery rate (FDR) estimation and possible contaminating proteins (e.g., keratin and bovine proteins from cell culture media), we identified a total of 2467 proteins at a 1% FDR threshold after removing isoforms from the same gene. Intensity-based absolute quantitation (iBAQ) was calculated.[24] Excluding proteins with missing quantification values resulted in 2156 proteins (Supporting Information). The raw data were then normalized (Figure 2A). Subsequently, we distinguished between identified and regulated proteins. Regulated proteins are those with an adj. p-value < 0.05. After applying the aforementioned criteria to our data set, we obtained a list of robustly regulated 558 proteins, which shows that diet-induced prediabetes alters the protein composition of GDEs (Figure 2A). All data, before applying the filtering criteria, are represented in a volcano plot that describes the level of significance and magnitude of changes observed, comparing the HD with the NCD group (Figure 2B). The dotted line in the plot represents the threshold of adj. p-value<0.05, and from that line above, each individual dot represents a protein within the 558 regulated ones.

Gene Ontology

To gain insights into the biological role of the 558 regulated proteins, we performed Gene Ontology and Kyoto Encyclopedia for Genes and Genomes (KEGG) enrichment analysis, which revealed that the vast majority of proteins were related

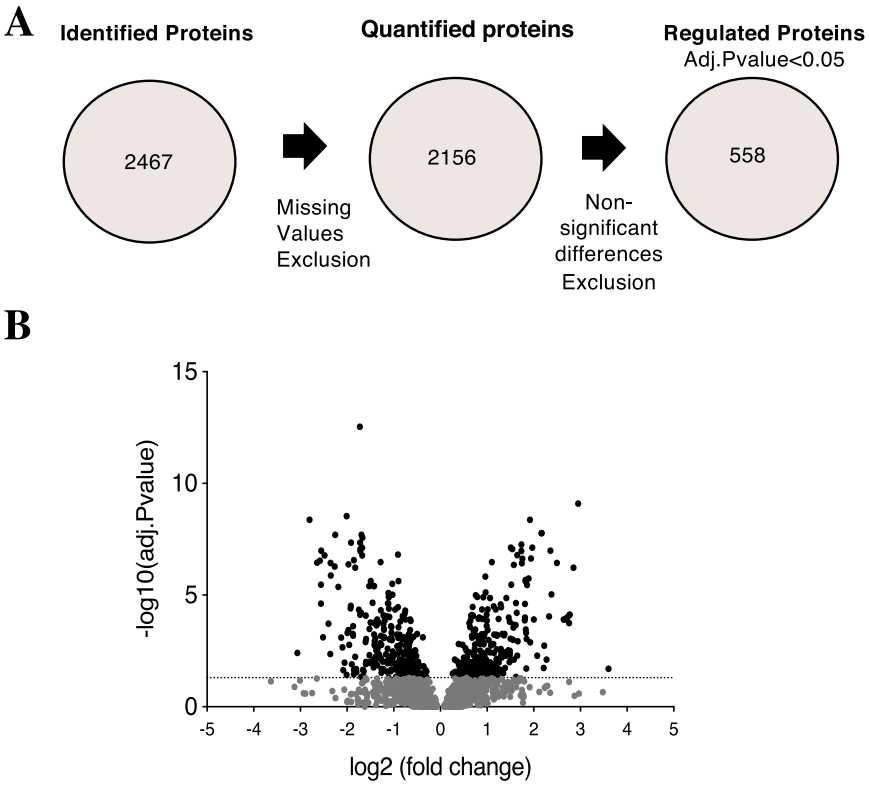

Figure 2. Study flow of proteomic approach for the characterization of GDE protein cargos. (A) Strategy used for the selection of proteins to be analyzed with confidence. (B) Volcano plot representing the fold change and adj. p-value in the GDE isolated from prediabetic mice and control groups. x-axis represents fold change, and y-axis represents adj. p-value. Dotted line sets the threshold of adj. p-value < 0.05. In gray are the nonregulated proteins, and in black are the 558 regulated proteins.

https://doi.org/10.1021/acs.jproteome.1c00353
J. Proteome Res. 2022, 21, 910–920

with metabolism. In terms of molecular function, enzyme activity (including isomerases, hydrolases, and oxidoreductase) shows up in the top of the list (Figure 3A). Most of the enriched pathways for gene ontology biological process emphasized lipid metabolism, highlighting fatty acid (FA) β-oxidation. Curiously, glycolysis-related and proteolysis in cellular protein catabolic processes-related proteins are mostly downregulated (Figure 3B). Considering KEGG pathway enrichment analysis, the affected proteins belong primarily to FA, carbohydrate, and amino acid metabolism. Interestingly, alcoholism-related proteins show up with great significance (Figure 3C). In terms of downregulated proteins, based on the KEGG analysis, the proteasome and focal adhesion proteins are markedly downregulated. Finally, to assess subcellular localization of the GDE protein cargo regulated by diet, we used gene ontology cellular component analysis and found that the majority of altered proteins are mitochondrial, followed by the cytosolic ones. Once again, proteasome-related proteins were downregulated (Figure 3D).

Cluster Analysis for GDE-Regulated Proteins

For a more detailed characterization of GDE proteome, we looked into the subset of proteins that were overly altered among groups. For that, we established an adj. p-value<0.0001 as cutoff (Figure 4A). The proteins with that significance are represented in the heatmap (Figure 4B). To gain insights into the protein−protein interaction of GDE-identified protein cargo, we used the STRING software to link some of the altered proteins and to display the level of relationship between them. The proteins that demonstrate a higher level of interaction are the ones related with the proteasome, including both α subunits (PSMA) and β (PSMB). Actin-related proteins, whose function is to maintain cellular integrity, also display relevant interactions. Moreover, network analysis highlights the strong tendency toward metabolic-related proteins (Figure S3). The fold change of all altered proteins varied up to twofold when comparing HD with NCD GDE. Within metabolic pathways, the altered proteins are mainly involved in nutrient metabolism, such as glucose, Fas, and amino acids. In addition, cell integrity, focal adhesion, and proteasome-related proteins are all downregulated (Figures 4C and S4). Key GDE proteins up- and downregulated by HD are also represented in their subcellular location (Figure 5). Noteworthy to mention, proteins related with carbohydrate metabolism, which ensures the supply of energy to the cells (PFKL, ALDOA, ALDOB, PGAM2, ENO1, and PGM5), with the tricarboxylic acid (TCA) cycle (DLST and IDH1); cholesterol homeostasis (ACAT1 and ACAT2); and proteasome (PSMA1, PSMA2, PSMA3, PSMA4, PSMA5, PSMA6, PSMA7, PSMB1, PSMB2, PSMB3, PSMB8, and PSMB10) are downregulated by HD. On the other hand, proteins related with lipid homeostasis (ACOT1 ACOT2, ACOT3, ACOT5, and ACOT6), FA mitochondrial β-oxidation (HDHA, ACADVL, ACADL, ECHS1, and ACAA2), very-long chain FA peroxisomal β-oxidation (ECH1 and ACOX1), amino acid metabolism (GSTA1 and GSTA2), and antioxidant defense (ALDH2, ALDH1B1, PRDX6, GSTA4, and GSTM2) are majorly upregulated. Table 1 describes all the proteins up- and downregulated according to their biological function.

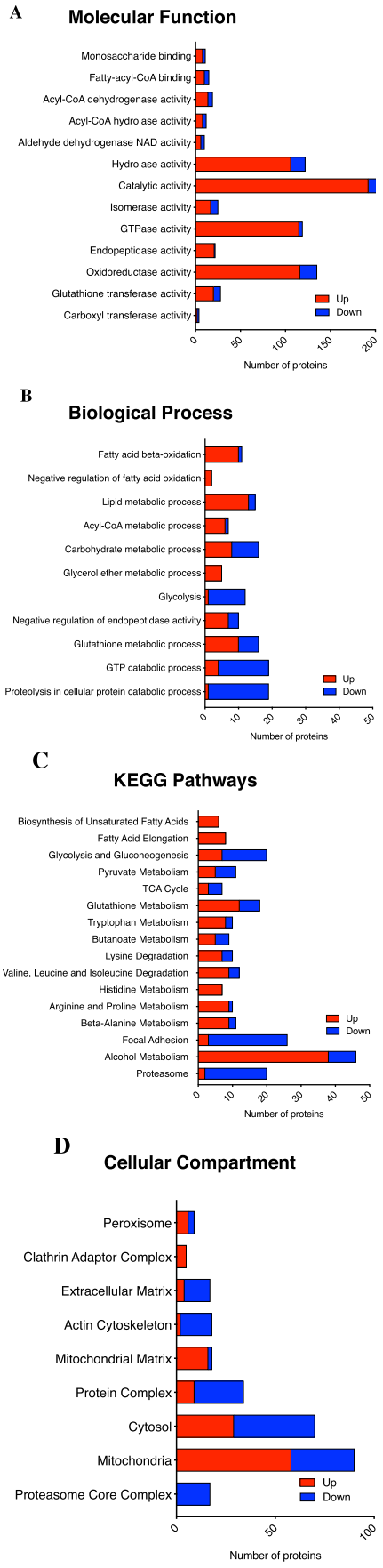

Figure 3. Characterization of prediabetic GDE by GO and KEGG enrichment analysis directly against mouse annotation according to

DISCUSSION

The relationship between diet composition and the incidence of metabolic disorders is a public health concern. One of the

https://doi.org/10.1021/acs.jproteome.1c00353
J. Proteome Res. 2022, 21, 910−920

Figure 3. continued

GO terms. (A) Molecular function analysis of the GDE identified proteins. GO enrichment analysis according to molecular function. (B) Analysis of the main biological process regulated by the proteins identified in the GDE. GO enrichment analysis according to the biological process. (C) KEGG enrichment analysis for the KEGG pathway. (D) GO enrichment analysis according to cellular compartment. On the left panels, changes are displayed as the number of proteins with increased (red) or decreased (blue) levels (horizontal axis).

first organs and by far the largest one to contact with food and its derivates is the gut, and as a consequence, it is where the first organismal response should be found.[25] Here, we report that GDE isolated from animals fed a HD, mimicking the western one, have a distinct proteome that strongly reflects the intestinal dysmetabolic milieu. We found numerous pathways associated with macronutrients altered in GDE isolated from HD-fed mice; of great relevance the ones related with lipidic and carbohydrate metabolic processes.

From the enrichment analysis, we observed that both glycolysis-gluconeogenesis and pyruvate pathways are within the most affected ones (Figure 3B). Rate-limiting enzymes for glycolysis were found to be less abundant, namely, hexokinase (HK) and PFKL, thus suggesting changes in sucrose utilization and lactate production. In accordance, in diabetic rats, phosphorylation of glucose is inhibited in tissues such as the heart, skeletal muscle, and liver.[26−28] Interestingly, in hearts from diabetic rats, PFK and HK downregulation is reverted by an oral antidiabetic drug—metformin.[29] We suggest that the observed decreased levels of PFKL in prediabetic GDEs are mirroring a similar downregulation in the small intestine of prediabetic mice; it is an early event in the progression of the disease.[30] Down in the glycolysis pathway, pyruvate dehydrogenase A1 (PDHA1), which belongs to the PDH complex, was upregulated in HD GDEs, indicating a possible compensation in the pathway given the importance of acetyl-CoA for the TCA cycle and for many other proteins and lipidic biochemical reactions. PDH is fundamental for metabolic flexibility, the ability of switching from carbohydrates to lipid fuel as energy sources, and the inability of cells to do so is an important hallmark of T2D.[31] Our results suggest that in the early stages of the disease, gut cells tackle the insult of HD feeding by changing the source of fuel. The decrease in glycolysis might be explained by the low amount of fibers provided by the diet because the percentage of fibers in HD is considerably reduced and in part replaced by sucrose. Likewise, fibers have a beneficial effect on NCD and HC mice by improving intestinal integrity, enhancing energy expenditure, and reducing inflammation.[32] In fact, because HD has increased sucrose, we envisage that sucrose is being directed to an alternative pathway, such as de novo lipogenesis, known to also occur in the gut.[33] Currently, high-fructose corn syrup consumption is seen as one of the main culprits of the obesity epidemics we are facing, and as a consequence, there is a growing interest in understanding how different sugars are differentially metabolized by the body.[34−37] While for many years the liver has been seen as the main organ for fructose metabolization, recently the intestine came into the picture. Studies in mice and humans have shown a capacity for intestinal fructose metabolism coupled to intestinal gluconeogenesis.[38−40] In light of these findings, the intestine would be the first organ to metabolize

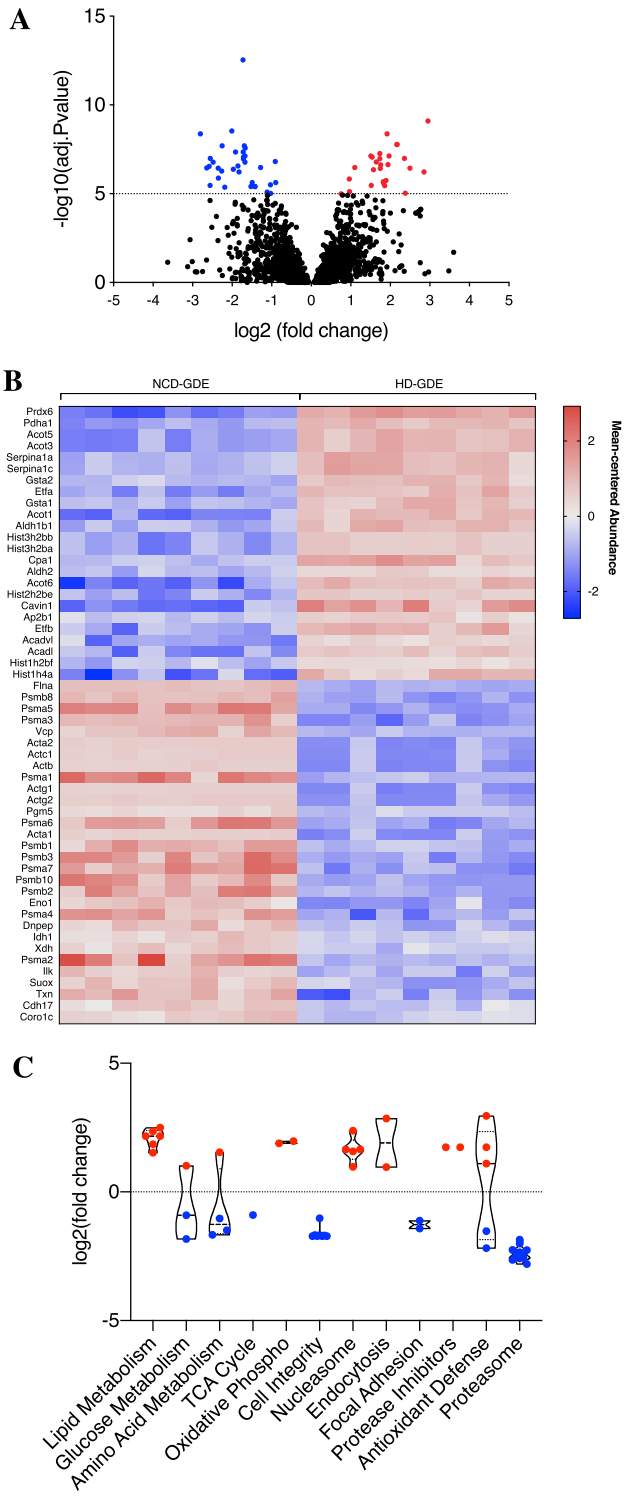

Figure 4. Cluster analysis of the top 50 altered proteins of GDE in prediabetic mice. (A) Volcano plot representing the fold change and adj. *p*-value of GDE proteins isolated from prediabetic mice and control groups. *x*-axis represents fold change, and *y*-axis represents adj. *p*-value. Dotted line sets the threshold of adj. *p*-value < 0.0001, highlighting the most altered proteins in GDE from HD comparing with GDE from NCD. In blue are the most downregulated proteins and in red the most upregulated. (B) Heatmap representing mean-centered abundance of the most altered proteins decorated in the previous volcano plot. (C) Violin plot demonstrating the fold changes of the most altered proteins and correspondent cellular functions. Cellular metabolic process (GO) represented in green.

https://doi.org/10.1021/acs.jproteome.1c00353
J. Proteome Res. 2022, 21, 910−920

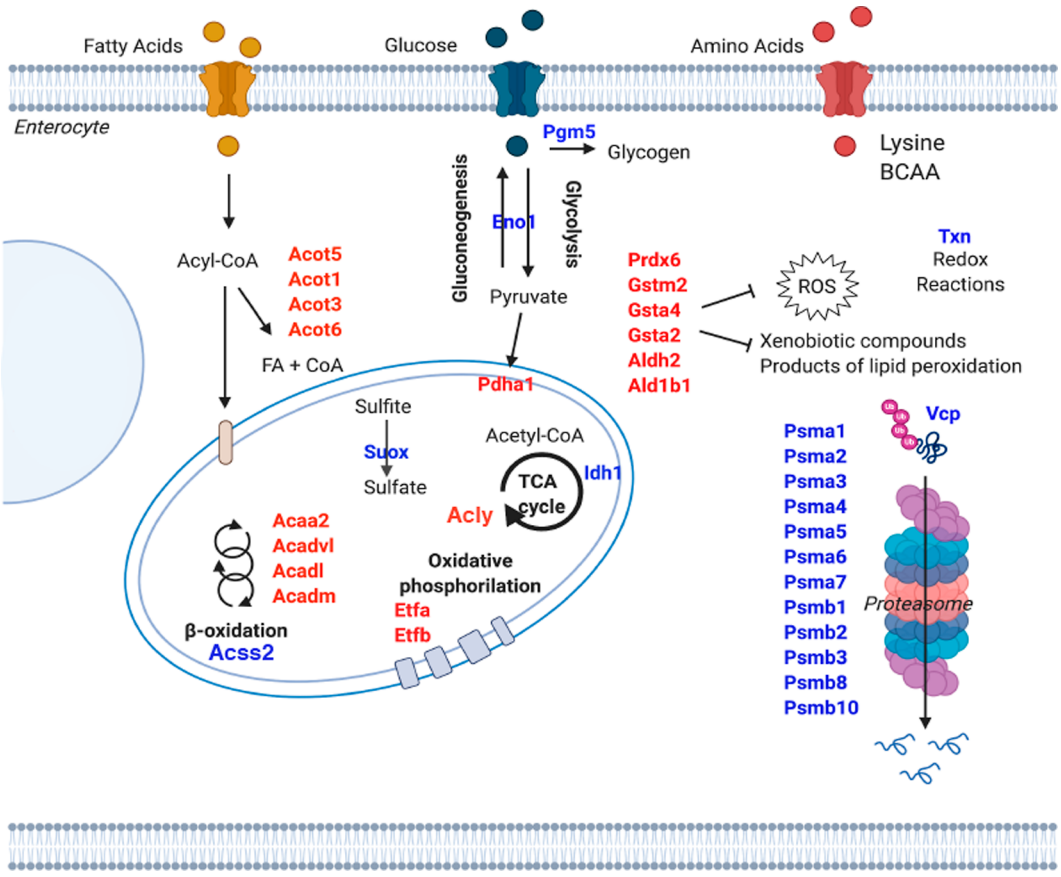

Figure 5. Overview of prediabetes impact on the GDE proteome. The identified proteins with higher differential expression are represented in the image according to their function and estimated subcellular localization. Red color for proteins upregulated and blue color for proteins downregulated in small intestine-derived EV of mice fed with HD compared with controls, mice fed with NCD. ROS; TCA. Image done in BioRender.

fructose, thus controlling portal vein load of this particular sugar. Importantly, besides increased glucose, HD also presents increased fructose in a ratio of 1:1 (sucrose/fructose), and the fact that PFKL was decreased in GDE from animals exposed to this diet may be partially explained by an increased usage of this enzyme by the cells in the gut due to diet fructose overload.

In accordance with the high lipidic content present in the HD, we observed that lipid metabolism (biosynthesis of unsaturated FA and FA elongation) is vastly altered. The excess of fat in the diet is known to cause increased FA uptake, which can be either metabolized for the production of energy or, when in excess, will be stored. Several proteins involved in mitochondrial β-oxidation (HADHA, ACADVL, ACADL, ECH1, and ECHS1), which generates acetyl-CoA to feed the TCA cycle, and peroxisome β-oxidation (ECH1 and ACOX1), major FAs degradative pathway, are upregulated in GDE by HD, suggesting that FAs are favored as an energy source over glucose (Figure 5). In addition, over-activation of lipid metabolism-related pathways is a common feature of obesity and T2D, leading to a state of hyperglycemia.[41−43] Moreover, a family of acyl-CoA thioesterases (ACOTs) were particularly upregulated; these are intermediaries in the decision whether FAs are directed to the TCA cycle or stored (Figures 5 and S4).[44,45] Altogether, this suggests that HD shifts the burden of energy provision from carbohydrates toward fat derived from diet because ACSS2 (a protein that conducts FAs to the TCA cycle) is downregulated and PDHA1 (which provides a link between glycolysis, TCA cycle, and lipogenesis) is upregulated in order to ensure the energetic need of the cell. Based on the recent literature, obesity-induced activation of ACOTs directs FAs toward triglyceride synthesis for incorporation into chylomicrons or VLDL particles.[46] Noteworthy, some studies consider activation of ACOTs protective against FA oversupply, slowing the flux of FAs to downstream metabolic pathways.[47−49] Whether this is the case in the gut, needs to be further explored. Additionally, intestinal cells in the HD model appear to prioritize the production of energy from FAs instead of carbohydrates. This is shown by the upregulation of ATP-citrate lyase, an enzyme responsible for the conversion of citrate into acetyl-CoA—the first step in DNL. Overall, the major enzymes found altered within the gut EVs are very much responsible for regulating acetyl-CoA levels in the cells, given that this molecule is a fundamental node in the metabolism, and in the future, it would be of major interest to quantify it in enterocytes.

Increased FA oxidation promotes mitochondrial dysfunction, as well as FA peroxidation and glucose dysmetabolism, altogether leading to reactive oxygen species (ROS) accumulation to pernicious levels.[50] Oxidative stress is implicated in various diseases including diabetes.[51] We observed several proteins involved in antioxidant defense mechanisms, such as removal of free radicals (PRDX6) and elimination of xenobiotic compounds and products of lipid peroxidation (GSTA4 and GSTM2) upregulated in HD-GDE, suggesting an activation of an antioxidant response in the gut cells (Figure

https://doi.org/10.1021/acs.jproteome.1c00353
J. Proteome Res. 2022, 21, 910−920

Table 1. Regulated Proteins According to Their Biological Function[a]

biological function	up	down
	Lipid Metabolism	
mitochondrial β-oxidation	ACADVL; ACADL	
lipid Homeostasis	ACOT1; ACOT2; ACOT3; ACOT5; ACOT6	
	Glucose Metabolism	
glycolysis		ENO1; PGM5
conversion of pyruvate to acetyl-CoA	PDHA1	
	Amino Acid Metabolism	
C-terminal amino acid release	CPA1	
protein degradation		VCP
peptide metabolism		DNPEP
purine Metabolism		XDH
TCA cycle		IDH1
oxidative phosphorylation	ETFA; ETFB	
cell Integrity		ACTA1; ACTA2; ACTB; ACTC1; ACTG1; ACTG2; CORO1C; FLNA
nucleosome	HIST1H4A; HIST3H2BB; HIST3H2BA; HIST2H2BE; HIST1H2BF	
	Endocytosis	
caveolar endocytosis	CAVIN1	
clathrin-dependent endocytosis	AP2B1	
focal adhesion		ILK; CDH17
protease inhibitor	SERPINA1A; SERPINA1C	
antioxidant defense	PRDX6; GSTA4; GSTA1; GSTA2; ALDH2; ALDH1B1	TXN; SUOX
proteasome		PSMA1; PSMA2; PSMA3; PSMA4; PSMA5; PSMA6; PSMA7; PSMB1; PSMB2; PSMB3;PSMB8; PSMB10

[a]Biological function of the main up- and downregulated proteins in HD-GDE compared with NCD-GDE by proteomics.

5). Consistent with our model, the presence of numerous isoforms of the aldehyde dehydrogenase (ALDH) family was upregulated in HD-derived GDE. ALDHs are a family of oxidizing enzymes responsible for cellular detoxification by oxidation of biogenic and xenogeneic aldehydes that accumulate through metabolism.[52] In particular, we highlight ALDH1B1 due to its ability to metabolize acetaldehyde and maintain glucose homeostasis.[53] Of interest, ALDH2 has been explored as a pharmacological target, due to its role in cellular damage defense against oxidative stress induced by pathological conditions, for instances high glucose.[54] Other important pathway when it comes to defenses against oxidative stress is the glutathione metabolism (Figure 3C), where we found nine upregulated proteins, suggesting that as early as the food gets to the small intestine, the organism starts to fight the deleterious effects of oxidative stress.

Besides glucose and FAs, amino acids, in particular lysine, also play important roles in providing energy to gut epithelial cells[55] (Figure 3C). Lysine, whose pathway we see affected in HD-GDE, mediates protein biosynthesis, such as of carnitine, a key factor in FA metabolism.[56] Interestingly, carnitine deficiency due to poor lysine diet induces triglyceride accumulation.[57] Another interesting amino acid in the context of prediabetes is L-arginine. Out of the 10 regulated proteins identified in the arginine and proline metabolism (Figure 3C), nine are upregulated in agreement with the idea that arginine, a well-known insulin secretagogue, also works in the intestine to stimulate the release of the glucagon-like peptide 1, which contributes to the characteristic prediabetic hyperinsulinemia.[58−60]

Evidence that the HD not only induces obesity but also a general pathological state arises from the massive alteration of proteasome-related proteins. The proteasome is recognized as an important target in many diseases.[61] Our data showed downregulation of proteasome proteins, which is consistent with decreased proteasome function reported in a broad array of chronic diseases (Figures 3C and 5). One hypothesis is that the decreased content of proteasome proteins in prediabetic GDE mirror in the cell of origin. Alternatively, the GDE-producing cells can be overutilizing the proteasome to counteract the deleterious effects of oxidative stress, resulting in lower packaging of proteasome proteins in GDEs.

The present study is the first comprehensive analysis of GDE protein content. We found that diet composition strongly modulates the GDE proteomic profile. Several lines of evidence support a model in which the metabolic alterations induced by the HD are translated in a similar manner in alterations in GDE protein cargo. These results bring light into the important modification taking place in the small intestine and how it translates into GDE content. We propose that future studies should focus on whether GDE can act in local and distant cellular targets and mediate prediabetes. We also propose that the analysis of GDE in biofluids may represent a strategy to noninvasively detect metabolic modifications in the gut linked with prediabetes and potentially be employed as an early diagnose and follow-up for prediabetic patients.

MATERIAL AND METHODS

Animals

Male C57Bl/6J mice were housed in a temperature-controlled room, in a 12 h light/dark cycle. For induction of prediabetic phenotype, C57BL/6J mice started on a high-fat diet at 6 weeks of age, with free access to food and water, for 12 weeks.

https://doi.org/10.1021/acs.jproteome.1c00353
J. Proteome Res. 2022, 21, 910−920

HD (OpenSource Diet, D12331) composition is 16.5% protein, 25.5% carbohydrate, and 58% fat with 13% addition of sucrose. The control NCD (special diets services, RM3) composition is 26.51% proteins, 62.14% carbohydrates, and 11.35% fat and no sucrose. At 18 weeks of age, 12 weeks of diet, mice were sacrificed. Mice were anesthetized using 2% isoflurane. Mice were sacrificed after 12 h of fasting, with a previous feeding period of 2 h, with a previous 8 h of fasting. Blood, liver, and small intestine were collected from prediabetic mice and respective controls. All animals were treated according with National and European Union Directive for Protection of Vertebrates.

Glucose Tolerance Test

At week 11 of the diet, glucose tolerance test (GTT) was performed. Mice were fasted overnight and weighed in the morning. Mice were then given an intra-peritoneal injection of a glucose solution (20% m/v—Sigma-Aldrich) at 2 g/kg body weight. Serum blood glucose levels were measured at 0, 15, 30, 60, 90, and 120 min after injection. Blood glucose levels were measured using an OneTouch Ultra glucose meter (LifeScan Inc).

Small Intestine Histology

After sacrifice, the liver and small intestine were washed in phosphate-buffered saline (PBS) and fixed for histology, and a portion of small intestine was snap-frozen in liquid nitrogen for later analysis by western blot. The clean gut was placed in 2% paraformaldehyde with 20% sucrose, overnight at 4 °C; washed three times in PBS, 10 min each; transferred to 30% sucrose for 2 h at 4 °C; and left overnight at 4 °C in OCT embedding matrix with 30% sucrose (1:1). In the following day, tissues were embedded in 20% sucrose (1:4) + OCT (3:4) in the presence of dry ice and immediately stored at −80 °C. Consequently, tissues were sliced into 6 μm sections in the cryostat and stored at −80 °C for following applications. Gut samples were used for CD81 staining and liver samples for hematoxylin−eosin staining.

Exosome Isolation and Nanoparticle Tracking Analysis

After sacrifice, the small intestine was removed, washed with PBS, and cultured overnight, at 37 °C and 5% CO_2, in RPMI medium (Sigma) supplemented with 1% penicillin/streptomycin and 10% fetal bovine serum EV-free to avoid contaminations from serum EVs. In the following day, the medium was collected. The conditioned medium was submitted to two initial centrifugations (10 min, 500*g* and 20 min, 3000*g*) to remove any suspended or dead cells in the medium. To remove large EVs, media were centrifuged (20 min, 12,000*g*) and the pellet was discarded. The supernatant enriched in small EVs was again centrifuged (2 h 20 min, 100,000*g*), and the EVs enriched pellet was collected. For sucrose cushion purification, this pellet was resuspended in 14 mL of filtered PBS (Corning 15313581, NY, US) and added to the top of 4 mL of sucrose solution (D_2O containing 1.2 g of protease-free sucrose and 96 mg of Tris base adjusted to pH 7.4). A new ultracentrifugation was performed (1 h 10 min, 100,000*g*), after which 4 mL of the sucrose fraction was collected using a 18 G needle placed at the bottom of the ultracentrifugation tube (away from the pellet). Finally, 16 mL of PBS were added to the collected sucrose/EVs solution and an overnight (16 h, 100,000*g*) ultracentrifugation was performed. The pellet containing the isolated EVs was resuspended in filtered PBS. The concentration and size of EVs were analyzed in a NanoSight NS300 (NS3000) system equipped with a blue laser (405 nm) according to the manufacturer's instructions. EVs were diluted 1:1000 in filtered sterile PBS. Each sample analysis was conducted for 90 s and measured five times using Nanosight automatic analysis settings. The software calculated the size distribution in nanometers and the concentration in number of particles per milliliter.

Western Blotting

Protein extracts for western blot analysis were obtained using cold lysis buffer [20 mM Tris-HCl pH 7.4, 5 mM ethylenediaminetetraacetic acid (EDTA) pH 8.0, 1% Triton-X 100, 2 mM Na_3VO_4, 100 mM NaF, 10 mM $Na_4P_2O_7$] in the presence of protease inhibitors (cOmplete, Mini, EDTA-free protein inhibitor cocktail tablets, Roche, Sigma). Gut tissue and GDE were homogenized in the lysis buffer and sonicated three times for 30 s each at 10 μm amplitude and incubated on ice between each sonication step. Lysates were centrifuged at 18,000*g* for 10 min at 4 °C. The soluble fraction was collected and protein concentration was determined using the PierceTM BCA Protein Assay kit (Thermo Fisher). For protein expression analysis, total protein was mixed with sample buffer [250 mM Tris−HCl pH 6.8, 8% sodium dodecyl sulfate (SDS), 40% glycerol, 8% β-mercaptoethanol, bromophenol] before being denaturated at 95 °C for 10 min. Samples were then resolved by an 8% sodium dodecyl sulfate (SDS)-polyacrylamide gel electrophoresis. Proteins were subsequently electrotransferred to a polyvinylidene fluoride (PVDF) membrane (immobilon-P membrane, PVDF, Millipore) for 20 min at 25 mA and 2,5 mV in a Trans-Blot Turbo Transfer System (BioRad). Membranes were blocked for 1 h at room temperature with 3% BSA (Thermo Fisher) in tris-buffered saline with 0.1% Tween (TBS-T) (blocking solution). Membranes were incubated overnight at 4 °C, with CD63 antibody (Santa Cruz Biotechnology) prepared in 3% BSA in TBS-T, diluted 1:1000. Membranes were washed three times with TBS-T and incubated for 1 h at RT with the secondary antibody anti-rabbit antibody diluted 1:5000 (Santa Cruz Biotechnology). Blots were developed with ECL (ECL Prime, GE Healthcare) according to manufacturer's instructions. ChemiDoc Touch (Biorad) was used to detect chemiluminescence. Band intensities were quantified using ImageLab software and compared to β-actin.

Nano-LC−MSMS Analysis

Peptide samples were analyzed by nano-LC−MSMS (Dionex RSLCnano 3000) coupled to a Q-Exactive Orbitrap mass spectrometer (Thermo Scientific). Briefly, 5 μL of sample was loaded onto a custom-made fused capillary precolumn (2 cm length, 360 μm OD, 75 μm ID) with a flow of 5 μL per min for 7 min. Trapped peptides were separated on a custom-made fused capillary column (20 cm length, 360 μm outer diameter, 75 μm inner diameter) packed with ReproSil Pur C18 3-μm resin (Dr. Maish, Ammerbuch-Entringen, Germany) with a flow of 300 nL per minute using a linear gradient from 92% A (0.1% formic acid) to 28% B (0.1% formic acid in 100 acetonitrile) over 93 min, followed by a linear gradient from 28% B to 35% B over 20 min at a flowrate of 300 nl per minute. Mass spectra were recorded in the positive ion mode applying automatic data-dependent switch between one Orbitrap survey MS scan in the mass range of 400−1200 *m/z*, followed by HCD fragmentation and Orbitrap detection of the 15 most intense ions observed in the MS scan. AGC target values in the Orbitrap for MS and MSMS scans were 1,000,000

https://doi.org/10.1021/acs.jproteome.1c00353
J. Proteome Res. 2022, 21, 910−920

ions at a resolution of 70,000 at m/z 200 for MS scans and 25,000 ions at m/z 200 for MSMS scans. Peptide fragmentation in the HCD cell was performed at normalized collision energy of 31 eV. Ion selection threshold was set to 5000 ions for MSMS analysis, and maximum injection time was 100 ms for MS scans and 200 ms for MSMS scans. Selected sequenced ions were dynamically excluded for 60 s.

MSMS Analysis

Mass accuracy was set to 5 ppm on the peptide level and 10 Da on the fragment ions. A maximum of four missed cleavages were used. Carbamidomethyl was set as a fixed modification. M oxidation, N-terminal protein acetyl, Q deamidation, and N deamidation were set as variable modifications. The MSMS data were searched against all reviewed mouse proteins from UniProt with concatenation of all the sequences in reverse, maintaining only lysine and arginine in place. The data were searched and quantified with both MaxQuant[62] and VEMS.[63]

STATISTICAL ANALYSIS

Data are presented as means ± SEM. GTT curves, bar plots, volcano plots, heatmap, and linear regression analyses were done using GraphPad Prism 8 (GraphPad Software). Difference significance was calculated through unpaired student's-t tests with Welch's correction; one-way ANOVA followed by Tukey–Kramer multiple comparison tests. Differences were accepted as statistically significant at $p < 0.05$.

ASSOCIATED CONTENT

Supporting Information

The Supporting Information is available free of charge at https://pubs.acs.org/doi/10.1021/acs.jproteome.1c00353.

> Full western blot images corresponding to main Figure 1G; study flow of the proteomic approach for the characterization of GDE protein cargos; schematic representation of the detailed protocol used for the isolation of GDE; schematic representation of the experimental process of analysis of GDE; bar plot indicating the number of proteins uniquely identified from different species when searched against all proteins from all species in UniProt; LB-agar (without antibiotics) Petri dish after 24 after hours of inoculation with media where guts were deposited overnight at 37 °C prior to EV isolation; protein–protein interaction network; individual protein alteration levels according to its biological function; and data plots demonstrating the log fold changes of each protein in the image in accordance to its related pathway (PDF)

AUTHOR INFORMATION

Corresponding Authors

Bruno Costa-Silva − *Champalimaud Research, Champalimaud Centre for the Unknown, 1400-038 Lisbon, Portugal*; Email: bruno.costa-silva@research.fchampalimaud.org

Maria Paula Macedo − *Chronic Diseases Research Centre, CEDOC, NOVA Medical School, (NMS/FCM), Lisbon 1169-056, Portugal; APDP-ERC Portuguese Diabetes Association Education and Research Centre, Lisbon 1250-189, Portugal; Departament of Medical Sciences, University of Aveiro, Aveiro 3810-193, Portugal*; Phone: (+351) 21 880 3017; Email: paula.macedo@nms.unl.pt; Fax: (+351) 21 880 3028

Authors

Inês Ferreira − *Chronic Diseases Research Centre, CEDOC, NOVA Medical School, (NMS/FCM), Lisbon 1169-056, Portugal; Bioengineering—Cell Therapies and Regenerative Medicine PhD Program, Instituto Superior Técnico, University of Lisbon, Lisbon 1049-001, Portugal; Champalimaud Research, Champalimaud Centre for the Unknown, 1400-038 Lisbon, Portugal*

Rita Machado de Oliveira − *Chronic Diseases Research Centre, CEDOC, NOVA Medical School, (NMS/FCM), Lisbon 1169-056, Portugal*; orcid.org/0000-0002-0970-4501

Ana Sofia Carvalho − *Chronic Diseases Research Centre, CEDOC, NOVA Medical School, (NMS/FCM), Lisbon 1169-056, Portugal*

Akiko Teshima − *Chronic Diseases Research Centre, CEDOC, NOVA Medical School, (NMS/FCM), Lisbon 1169-056, Portugal*

Hans Christian Beck − *Centre for Clinical Proteomics, Department of Clinical Biochemistry and Pharmacology, Odense University Hospital, Odense 5000, Denmark*

Rune Matthiesen − *Chronic Diseases Research Centre, CEDOC, NOVA Medical School, (NMS/FCM), Lisbon 1169-056, Portugal*; orcid.org/0000-0002-6353-2616

Complete contact information is available at: https://pubs.acs.org/10.1021/acs.jproteome.1c00353

Author Contributions

¶I.F. and R.M.O. contributed equally as first authors. B.C.-S. and M.P.M. contributed equally as last authors. I.F. and R.M.O. carried out the animal model of disease, western blotting, and drafted the manuscript. I.F. did the isolation of the EVs and characterization by NTA, gut histology, and performed bioinformatics analysis, together with R.M., for graphical representation. A.S.C. prepared GDE for MS analysis and R.M. was responsible for the MS analysis and bioinformatics. MS was performed by H.C.B. M.P.M. and B.C.-S. conceived the study, participated in its design and coordination, and edited the manuscript. All authors read and approved the final manuscript.

Notes

The authors declare the following competing financial interest(s): Maria Paula Macedo serves on the advisory board for Gilead Sciences.

ACKNOWLEDGMENTS

This work was supported by the Fundação para a Ciência e Tecnologia (grant no. PTDC/MEC-MET/29314/2017), iNOVA4Health UIDB/Multi/04462/2020, and Programa Gilead GÉNESE—Edição de 2019 awarded to M.P.M., R.M.O., and B.C.-S. I.F. is a recipient of Fundação para a Ciência e Tecnologia fellowship (PD/BD/114044/2015). A.T. is a recipient of the European Foundation for the Study of Diabetes and Japanese Diabetes Society Reciprocal Travel Research Fellowship Programme.

REFERENCES

(1) IDF. *IDF Diabetes Atlas*, 9th ed.; IDF, 2019; p 168.

(2) Rubino, F.; Nathan, D. M.; Eckel, R. H.; Schauer, P. R.; Alberti, K. G. M. M.; Zimmet, P. Z.; et al. Metabolic surgery in the treatment algorithm for type 2 diabetes: A joint statement by international diabetes organizations. *Diabetes Care* **2016**, *39*, 861−877.
(3) Aminian, A.; Vidal, J.; Salminen, P.; Still, C. D.; Nor Hanipah, Z.; Sharma, G.; et al. Late Relapse of Diabetes After Bariatric Surgery: Not Rare, but Not a Failure. *Diabetes Care* **2020**, *43*, 534−540.
(4) Petersen, M. C.; Shulman, G. I. Mechanisms of insulin action and insulin resistance. *Physiol. Rev.* **2018**, *98*, 2133−2223.
(5) Tabák, A. G.; Herder, C.; Rathmann, W.; Brunner, E. J.; Kivimäki, M. Prediabetes: A high-risk state for diabetes development. *Lancet* **2012**, *379*, 2279−2290.
(6) Hamdy, O.; Tasabehji, M. W.; Elseaidy, T.; Tomah, S.; Ashrafzadeh, S.; Mottalib, A. Fat Versus Carbohydrate-Based Energy-Restricted Diets for Weight Loss in Patients With Type 2 Diabetes. *Curr. Diabetes Rep.* **2018**, *18*, 128.
(7) Hooten, N. N.; Evans, M. K. Extracellular vesicles as signaling mediators in type 2 diabetes mellitus. *Am. J. Physiol. Cell Physiol.* **2020**, *318* (6), C1189−C1199.
(8) Zhang, J.; Li, S.; Li, L.; Li, M.; Guo, C.; Yao, J.; et al. Exosome and Exosomal MicroRNA: Trafficking, Sorting, and Function. *Genomics, Proteomics Bioinf.* **2015**, *13*, 17−24.
(9) Théry, C.; Zitvogel, L.; Amigorena, S. Exosomes: composition; biogenesis and function. *Nat. Rev. Immunol.* **2002**, *2*, 569−579.
(10) Deng, Z.-b.; Poliakov, A.; Hardy, R. W.; Clements, R.; Liu, C.; Liu, Y.; et al. Adipose tissue exosome-like vesicles mediate activation of macrophage-induced insulin resistance. *Diabetes* **2009**, *58*, 2498−2505.
(11) Kranendonk, M. E. G.; Visseren, F. L. J.; Van Herwaarden, J. A.; Nolte-'t Hoen, E. N. M.; De Jager, W.; Wauben, M. H. M.; et al. Effect of extracellular vesicles of human adipose tissue on insulin signaling in liver and muscle cells. *Obesity* **2014**, *22*, 2216−2223.
(12) Povero, D.; Yamashita, H.; Ren, W.; Subramanian, M. G.; Myers, R. P.; Eguchi, A.; et al. Characterization and Proteome of Circulating Extracellular Vesicles as Potential Biomarkers for NASH. *Hepatol. Commun.* **2020**, *4*, 1263−1278.
(13) Chang, X.; Wang, S.-L.; Zhao, S.-B.; Shi, Y.-H.; Pan, P.; Gu, L.; et al. Extracellular vesicles with possible roles in gut intestinal tract homeostasis and IBD. *Mediators Inflammation* **2020**, *2020*, 1945832.
(14) Smythies, L. E.; Smythies, J. R. Exosomes in the gut. *Front. Immunol.* **2014**, *5*, 104.
(15) Hu, G.; Gong, A. Y.; Roth, A. L.; Huang, B. Q.; Ward, H. D.; Zhu, G.; et al. Release of Luminal Exosomes Contributes to TLR4-Mediated Epithelial Antimicrobial Defense. *PLoS Pathog.* **2013**, *9*, No. e1003261.
(16) Chelakkot, C.; Choi, Y.; Kim, D.-K.; Park, H. T.; Ghim, J.; Kwon, Y.; et al. Akkermansia muciniphila-derived extracellular vesicles influence gut permeability through the regulation of tight junctions. *Exp. Mol. Med.* **2018**, *50*, No. e450.
(17) Mallegol, J.; Van Niel, G.; Heyman, M. Phenotypic and functional characterization of intestinal epithelial exosomes. *Blood Cells, Mol., Dis.* **2005**, *35*, 11−16.
(18) Evers, S. S.; Sandoval, D. A.; Seeley, R. J. The Physiology and Molecular Underpinnings of the Effects of Bariatric Surgery on Obesity and Diabetes. *Annu. Rev. Physiol.* **2017**, *79*, 313−334.
(19) Singh, A.; Kota, S.; Singh, R. Bariatric surgery and diabetes remission: Who would have thought it? *Indian J. Endocrinol. Metab.* **2015**, *19*, 563−576.
(20) David, L. A.; Maurice, C. F.; Carmody, R. N.; Gootenberg, D. B.; Button, J. E.; Wolfe, B. E.; et al. Diet rapidly and reproducibly alters the human gut microbiome. *Nature* **2014**, *505*, 559−563.
(21) Burcelin, R.; Serino, M.; Chabo, C.; Blasco-Baque, V.; Amar, J. Gut microbiota and diabetes: From pathogenesis to therapeutic perspective. *Acta Diabetol.* **2011**, *48*, 257−273.
(22) Kowalski, G. M.; Bruce, C. R. The regulation of glucose metabolism: Implications and considerations for the assessment of glucose homeostasis in rodents. *Am. J. Physiol.: Endocrinol. Metab.* **2014**, *307*, E859−E871.
(23) Kalra, H.; Drummen, G. P.; Mathivanan, S. Focus on extracellular vesicles: Introducing the next small big thing. *Int. J. Mol. Sci.* **2016**, *17* (2), 170.
(24) Schwanhäusser, B.; Busse, D.; Li, N.; Dittmar, G.; Schuchhardt, J.; Wolf, J.; et al. Global quantification of mammalian gene expression control. *Nature* **2011**, *473*, 337−342.
(25) Abumrad, N. A.; Davidson, N. O. Role of the gut in lipid homeostasis. *Physiol. Rev.* **2012**, *92*, 1061−1085.
(26) Kipnis, D. M.; Cori, C. F. Studies of Tissue Permeability: The Penetration and Phosphorylation of 2-deosyglucose in the diaphragm of diabetic rats. *J. Biol. Chem.* **1960**, *235*, 3070−3075.
(27) Chernick, S. S.; Chaikoff, I. L.; Abraham, S. Localization of initial block in glucose metabolism in diabetic liver slices. *J. Biol. Chem.* **1951**, *193*, 793−802.
(28) Renold, A. E.; Hastings, A. B.; Nesbett, F. B. Studies on carbohydrate metabolism in rat liver slices. III. Utilization of glucose and fructose by liver from normal and diabetic animals. *J. Biol. Chem.* **1954**, *209*, 687−696.
(29) Da Silva, D.; Ausina, P.; Alencar, E. M.; Coelho, W. S.; Zancan, P.; Sola-Penna, M. Metformin reverses hexokinase and phospho-fructokinase downregulation and intracellular distribution in the heart of diabetic mice. *IUBMB Life* **2012**, *64*, 766−774.
(30) Randle, P. J.; Garland, P. B.; Hales, C. N.; Newsholme, E. A. The Glucose Fatty-Acid Cycle Its Role in Insulin Sensitivity and the Metabolic Disturbances of Diabetes Mellitus. *Lancet* **1963**, *281*, 785−789.
(31) Kelley, D. E.; Mandarino, L. J. Fuel selection in human skeletal muscle in insulin resistance: A reexamination. *Diabetes* **2000**, *49*, 677−683.
(32) Jangra, S.; Raja, S. K.; Sharma, R. K.; Pothuraju, R.; Mohanty, A. K. Ameliorative effect of fermentable fibres on adiposity and insulin resistance in C57BL/6 mice fed a high-fat and sucrose diet. *Food Funct.* **2019**, *10*, 3696−3705.
(33) Hoffman, S.; Alvares, D.; Adeli, K. Intestinal lipogenesis: How carbs turn on triglyceride production in the gut. *Curr. Opin. Clin. Nutr. Metab. Care* **2019**, *22*, 284−288.
(34) Febbraio, M. A.; Karin, M. "Sweet death": Fructose as a metabolic toxin that targets the gut-liver axis. *Cell Metab.* **2021**, *33* (12), 2316−2328.
(35) Herman, M. A.; Birnbaum, M. J. Molecular aspects of fructose metabolism and metabolic disease. *Cell Metab.* **2021**, *33* (12), 2329−2354.
(36) Silva, J. C. P.; Marques, C.; Martins, F. O.; Viegas, I.; Tavares, L.; Macedo, M. P.; Jones, J. G. Determining contributions of exogenous glucose and fructose to de novo fatty acid and glycerol synthesis in liver and adipose tissue. *Metab. Eng.* **2019**, *56*, 69−76.
(37) Delgado, T. C.; Martins, F. O.; Carvalho, F.; Gonçalves, A.; Scott, D. K.; O'Doherty, R.; Macedo, M. P.; Jones, J. G. 2H enrichment distribution of hepatic glycogen from 2H2O reveals the contribution of dietary fructose to glycogen synthesis. *Am. J. Physiol.: Endocrinol. Metab.* **2013**, *304*, E384−E391.
(38) Barosa, C.; Ribeiro, R. T.; Andrade, R.; Raposo, J. F.; Jones, J. G. Effects of Meal Fructose/Glucose Composition on Postprandial Glucose Appearance and Hepatic Glycogen Synthesis in Healthy Subjects. *Jpn. Clin. Med.* **2021**, *10*, 596.
(39) Jang, C.; Hui, S.; Lu, W.; Cowan, A. J.; Morscher, R. J.; Lee, G.; Liu, W.; Tesz, G. J.; Birnbaum, M. J.; Rabinowitz, J. D. The small intestine converts dietary fructose into glucose and organic acids. *Cell Metab.* **2018**, *27*, 351−361.
(40) Varga, V.; Murányi, Z.; Kurucz, A.; Marcolongo, P.; Benedetti, A.; Bánhegyi, G.; Margittai, É. Species-specific glucose-6-phosphatase activity in the small intestine-studies in three different mammalian models. *Int. J. Mol. Sci.* **2019**, *20*, 5039.
(41) Deng, W.-J.; Nie, S.; Dai, J.; Wu, J.-R.; Zeng, R. Proteome, Phosphoproteome, and Hydroxyproteome of Liver Mitochondria in Diabetic Rats at Early Pathogenic Stages. *Mol. Cell. Proteomics* **2010**, *9*, 100−116.
(42) Kanuri, B. N.; Rebello, S. C.; Pathak, P.; Agarwal, H.; Kanshana, J. S.; Awasthi, D.; et al. Glucose and lipid metabolism

https://doi.org/10.1021/acs.jproteome.1c00353
J. Proteome Res. 2022, 21, 910−920

alterations in liver and adipose tissue pre-dispose p47phox knockout mice to systemic insulin resistance. *Free Radical Res.* **2018**, *52*, 568−582.
(43) Knebel, B.; Hartwig, S.; Haas, J.; Lehr, S.; Goeddeke, S.; Susanto, F.; et al. Peroxisomes compensate hepatic lipid overflow in mice with fatty liver. *Biochim. Biophys. Acta* **2015**, *1851*, 965−976.
(44) Wang, F.; Wu, J.; Qiu, Z.; Ge, X.; Liu, X.; Zhang, C.; et al. ACOT1 expression is associated with poor prognosis in gastric adenocarcinoma. *Hum. Pathol.* **2018**, *77*, 35−44.
(45) Steensels, S.; Qiao, J.; Zhang, Y.; Maner-Smith, K. M.; Kika, N.; Holman, C. D.; Corey, K. E.; et al. Acyl-Coenzyme A Thioesterase 9 Traffics Mitochondrial Short-Chain Fatty Acids Toward De Novo Lipogenesis and Glucose Production in the Liver. *Hepatology* **2020**, *72*, 857−872.
(46) Alves-Bezerra, M.; Li, Y.; Acuña, M.; Ivanova, A. A.; Corey, K. E.; Ortlund, E. A.; et al. Thioesterase Superfamily Member 2 Promotes Hepatic VLDL Secretion by Channeling Fatty Acids Into Triglyceride Biosynthesis. *Hepatology* **2019**, *70*, 496−510.
(47) Yamaguchi, K.; Yang, L.; McCall, S.; Huang, J.; Yu, X. X.; Pandey, S. K.; et al. Inhibiting triglyceride synthesis improves hepatic steatosis but exacerbates liver damage and fibrosis in obese mice with nonalcoholic steatohepatitis. *Hepatology* **2007**, *45*, 1366−1374.
(48) Fujita, M.; Momose, A.; Ohtomo, T.; Nishinosono, A.; Tanonaka, K.; Toyoda, H.; et al. Upregulation of fatty acyl-CoA thioesterases in the heart and skeletal muscle of rats fed a high-fat diet. *Biol. Pharm. Bull.* **2011**, *34*, 87−91.
(49) Franklin, M. P.; Sathyanarayan, A.; Mashek, D. G. Acyl-CoA Thioesterase 1 (ACOT1) Regulates PPARα to Couple Fatty Acid Flux With Oxidative Capacity During Fasting. *Diabetes* **2017**, *66*, 2112−2123.
(50) Volpe, C. M. O.; Villar-Delfino, P. H.; Dos Anjos, P. M. F.; Nogueira-Machado, J. A. Cellular death, reactive oxygen species (ROS) and diabetic complications. *Cell Death Discovery* **2018**, *9*, 119.
(51) Forman, H. J.; Zhang, H. Targeting oxidative stress in disease: promise and limitations of antioxidant therapy. *Nat. Rev. Drug Discovery* **2021**, *20*, 689−709.
(52) Ahmed Laskar, A.; Younus, H. Aldehyde toxicity and metabolism: the role of aldehyde dehydrogenases in detoxification, drug resistance and carcinogenesis. *Drug Metab. Rev.* **2019**, *51*, 42−64.
(53) Yang, C. K.; Wang, X. K.; Liao, X. W.; Han, C. Y.; Yu, T. D.; Qin, W.; et al. Aldehyde dehydrogenase 1 (ALDH1) isoform expression and potential clinical implications in hepatocellular carcinoma. *PLoS One* **2017**, *12*, No. e0182208.
(54) Chen, C.-H.; Ferreira, J. C. B.; Gross, E. R.; Mochly-Rosen, D. Targeting aldehyde dehydrogenase 2: New therapeutic opportunities. *Physiol. Rev.* **2014**, *94*, 1−34.
(55) Van Goudoever, J. B.; Stoll, B.; Henry, J. F.; Burrin, D. G.; Reeds, P. J. Adaptive regulation of intestinal lysine metabolism. *Proc. Natl. Acad. Sci. U.S.A.* **2000**, *97*, 11620−11625.
(56) Azevedo, C.; Saiardi, A. Why always lysine? The ongoing tale of one of the most modified amino acids. *Adv. Biol. Regul.* **2016**, *60*, 144−150.
(57) Khan, L.; Bamji, M. S. Tissue Carnitine Deficiency due to Dietary Lysine Deficiency: Triglyceride Accumulation and Concomitant Impairment in Fatty Acid Oxidation. *J. Nutr.* **1979**, *109*, 24−31.
(58) Greenfield, J. R.; Farooqi, I. S.; Keogh, J. M.; Henning, E.; Habib, A. M.; Blackwood, A.; et al. Oral glutamine increases circulating glucagon-like peptide 1, glucagon, and insulin concentrations in lean, obese, and type 2 diabetic subjects. *Am. J. Clin. Nutr.* **2009**, *89*, 106−113.
(59) Holst, J. J. The physiology of glucagon-like peptide 1. *Physiol. Rev.* **2007**, *87*, 1409−1439.
(60) Baggio, L. L.; Drucker, D. J. Biology of incretins: GLP-1 and GIP. *Gastroenterology* **2007**, *132*, 2131−2157.
(61) Rousseau, A.; Bertolotti, A. Regulation of proteasome assembly and activity in health and disease. *Nat. Rev. Mol. Cell Biol.* **2018**, *19*, 697−712.
(62) Cox, J.; Mann, M. MaxQuant enables high peptide identification rates, individualized p.p.b.-range mass accuracies and proteome-wide protein quantification. *Nat. Biotechnol.* **2008**, *26*, 1367−1372.
(63) Carvalho, A. S.; Ribeiro, H.; Voabil, P.; Penque, D.; Jensen, O. N.; Molina, H.; et al. Global mass spectrometry and transcriptomics array based drug profiling provides novel insight into glucosamine induced endoplasmic reticulum stress. *Mol. Cell. Proteomics* **2014**, *13*, 3294−3307.

https://doi.org/10.1021/acs.jproteome.1c00353
J. Proteome Res. 2022, 21, 910−920